Cell Reports, Volume *31*

Supplemental Information

Assembly and Function of a Bioengineered Human Liver for Transplantation Generated Solely from Induced Pluripotent Stem Cells

Kazuki Takeishi, Alexandra Collin de l'Hortet, Yang Wang, Kan Handa, Jorge Guzman-Lepe, Kentaro Matsubara, Kazutoyo Morita, Sae Jang, Nils Haep, Rodrigo M. Florentino, Fangchao Yuan, Ken Fukumitsu, Kimimasa Tobita, Wendell Sun, Jonathan Franks, Evan R. Delgado, Erik M. Shapiro, Nicolas A. Fraunhoffer, Andrew W. Duncan, Hiroshi Yagi, Tomoji Mashimo, Ira J. Fox, and Alejandro Soto-Gutierrez

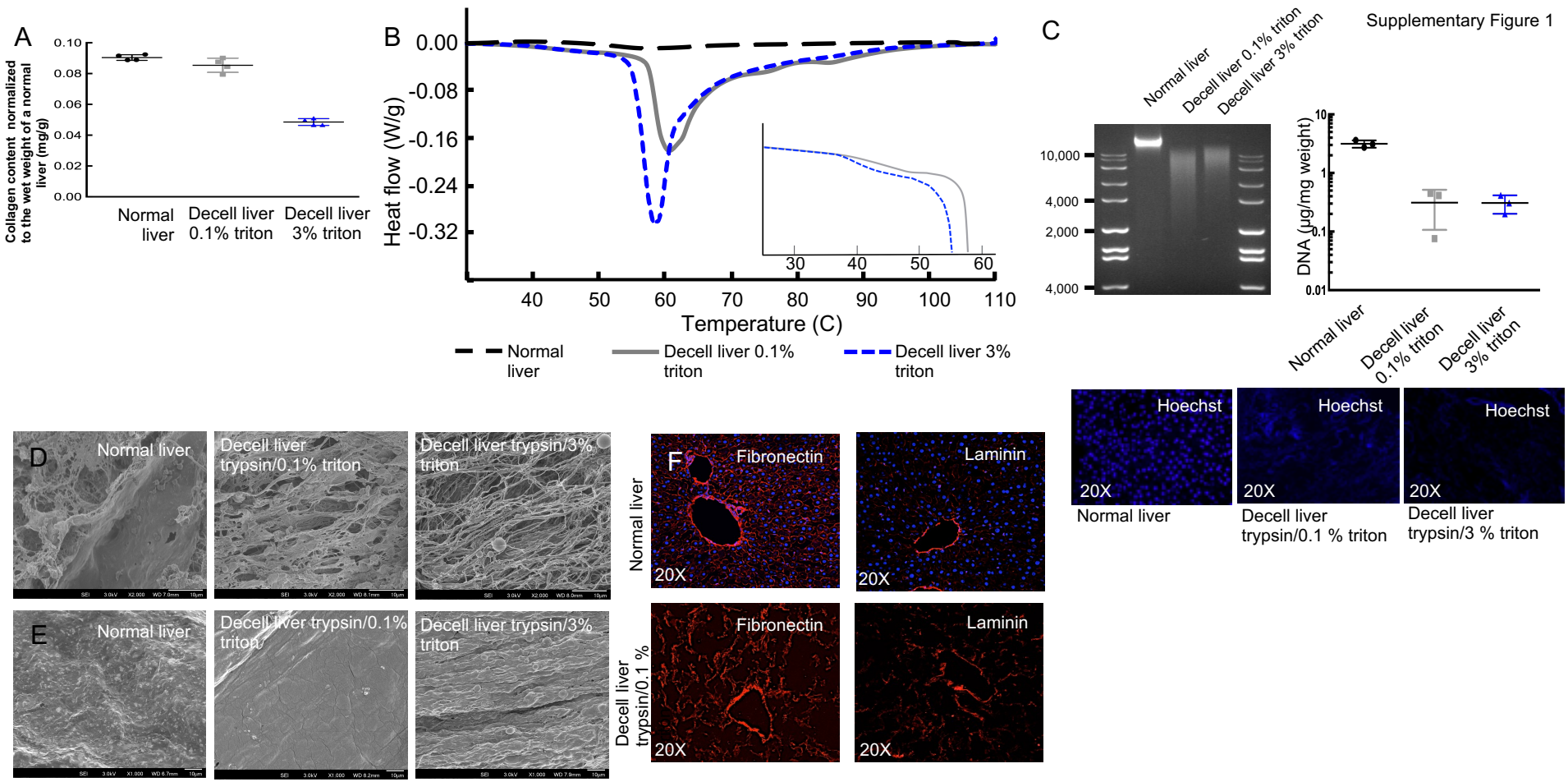

Supplemental Figure 1. Optimization and characterization of decellularized rat livers. Related to STAR Methods. (A) Hydroxyproline assay for collagen content of normal and decellularized rat liver using 3% and 0.1% triton X-100 solutions (n= 4). Bars represent the mean ± the S.D of four independent experiment. **(B)** Differential scanning calorimetry thermograms of normal liver (green) and decellularized liver using 3% (blue) and 0.1% (red) triton X-100 solutions. Samples were scanned at 3 °C/min between 2 °C and 125 °C. Plotted lines were the weight-averaged curves of four samples in each group. The inset shows the lower temperature shoulders of extracellular tissue matrices. The total denaturation enthalpy when using low concentrations of triton is 45.6 ± 5.0 J/g (n=4). The total denaturation enthalpy for extracellular matrices derived with 3.0% Triton X-100 is 55.8 ± 4.7 J/g (n= 4), a value that is significantly higher than that of the extracellular tissue matrix derived with 0.1% Triton X100 (p value=0.026 by Student's t-test) and is similar to purified collagen. **(C)** Electrophoresis on agarose gel and absorbance based nuclei acid analysis for DNA content of normal and decellularized rat liver using 3% and 0.1% triton X-100 solutions (0.1% vs 3%, P=0.999 by one-way ANOVA, Tukey-Kramer) (n= 3), Bars represent the mean ± SD of three independent experiment. Additionally, images of Hoechst staining (blue fluorescent dye) used to stain remnant DNA. **(D)** scanning electron microscope (SEM) images of extracellular matrix within the parenchyma and **(E)** glisson's capsule of normal liver and after liver decellularization. (F) Comparison of normal liver (top) and decellularized liver (bottom). Left to right: fibronectin (red) and laminin (red) staining. Sections were counterstained with DAPI (blue). Scale bars: 10 µm (D and E).

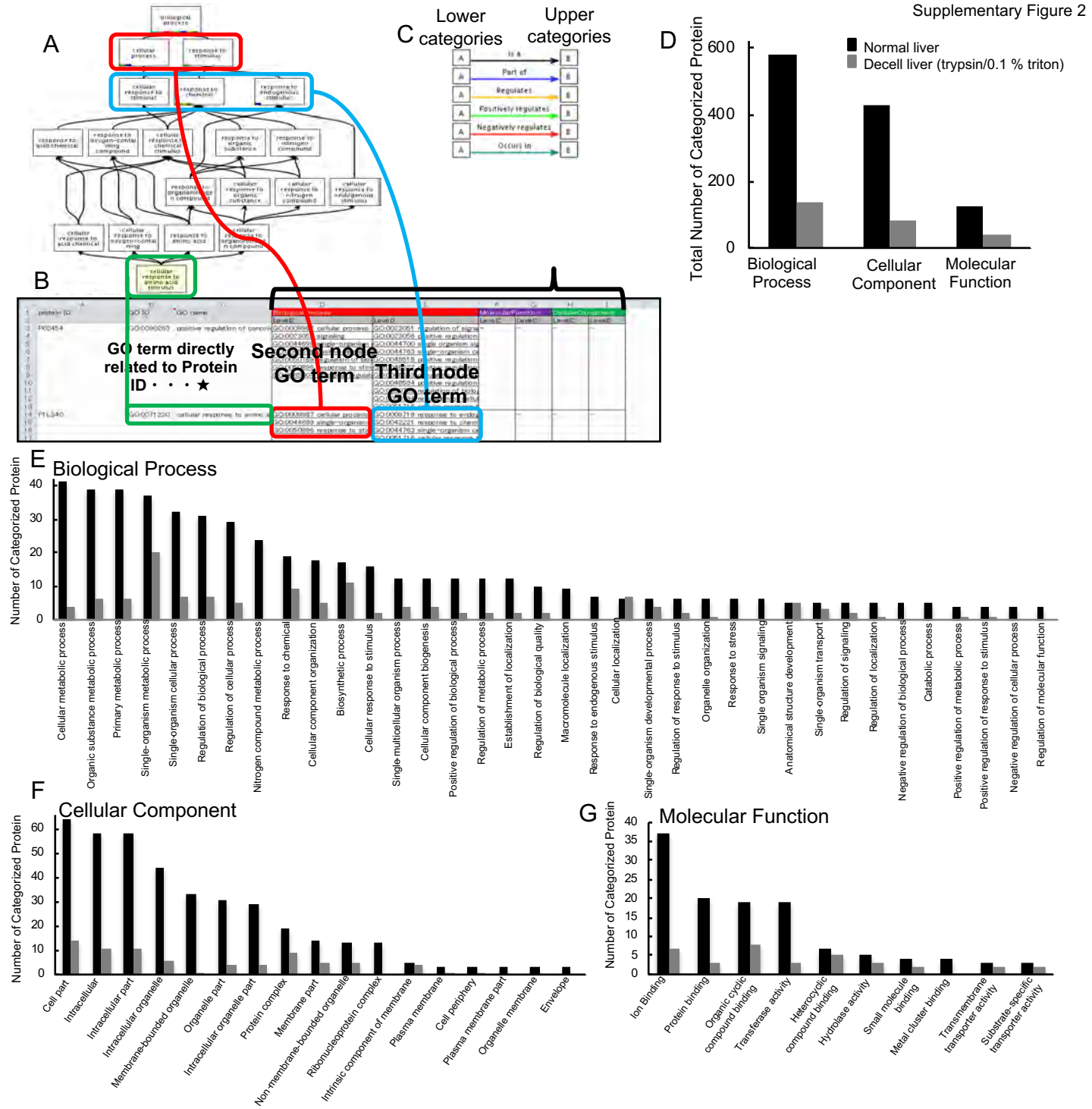

Supplemental Figure 2. Illustration representing the categorization of proteins detected in normal and decellularized rat livers. Related to STAR Methods. (A,B) Categorization of the three fundamental terms, e.g. biological process, cellular component and molecular function, for the identified proteins was performed with the assistance of Gene Ontology identification numbers (GO ID #s). After assigning a GO number, every GO term was categorized as to lower nodes for each three categories. **(C)** The ontology is not intended to represent a reaction pathway, but instead reflects conceptual categories of gene- product function. Note that a node may have more than one parent. A gene product can be associated with more than one node within the ontology, as illustrated, nevertheless, every GO term was finally categorized as three individual categories as described. (Figures were reference from QuickGO – http://www.ebi.ac.uk/QuickGO). **(D)** Categorization of the "biological process", "cellular component" and "molecular function" of the (909 proteins in normal liver and 141 proteins in decellularized liver) identified proteins was performed with the assistance of Gene Ontology (GO) identification numbers. The number of third node GO terms given for extracted proteins from either normal liver and decellularized liver were represented (n=1 per group). The number of categorized third node of GO terms is represented for the detected proteins from normal and decellularized liver for **(E)** Biological process, **(F)** Cellular components and **(G)** molecular function. Only categorized nodes with more than four GO terms are represented in the graphs.

A

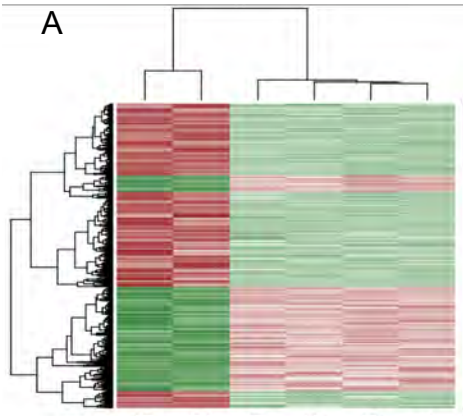

1 2 1 2 3 4

Human Adult liver | Human Fetal liver

Tissue ID	Sex	Age
A1	Female	16 years
A2	NF	28 years
F1	Female	19 weeks
F2	NF	21 weeks
F3	NF	22 weeks
F4	Female	18 weeks

Human Adult and fetal liver tissue used gene expression patterns using microarray analysis

B

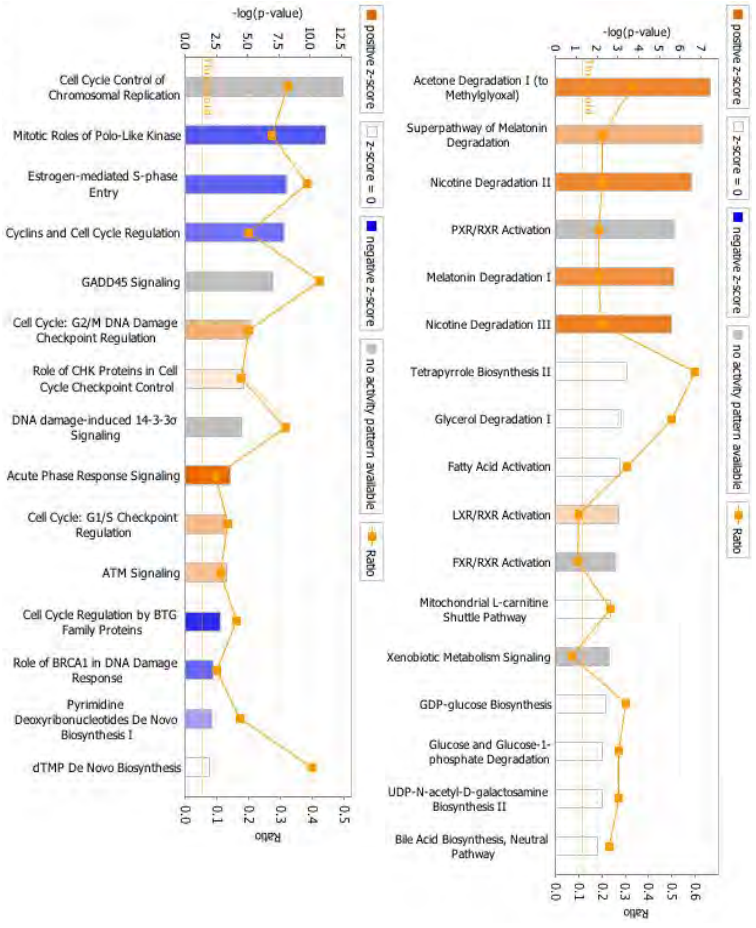

C

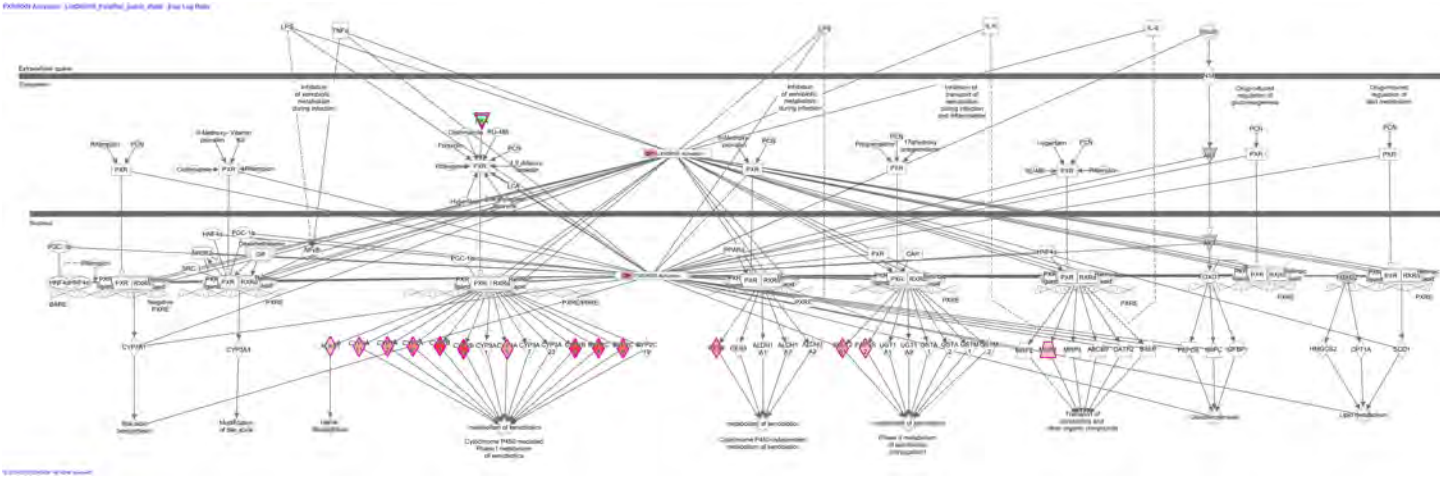

Supplemental Figure 3. Gene array of human adult and fetal livers. Related to Figure 1. (A) Heat map of statistically significant genes generated after applying the Expression Set data to oligo package (R software). Red, downregulated (726 genes); Green, upregulated (478 genes). **(B)** Cell cycle related canonical pathways that are altered significantly on transition from fetal to adult livers are identified using IPA (FC>2, $p<0.05$). Fetal to adult liver maturation results in statistically significant (FC>2, $p<0.05$) change in the metabolic pathways and the associated genes. **(C)** The top networks generated by IPA core analysis of the genes found significantly up-regulated in human adult liver when compared to human fetal liver, An IPA Core Analysis identified 3 ranked networks from the set of genes, which included some key gene networks of interest (lipid metabolism, transport and metabolism of xenobiotics, bile acid biosynthesis and gluconeogenesis).

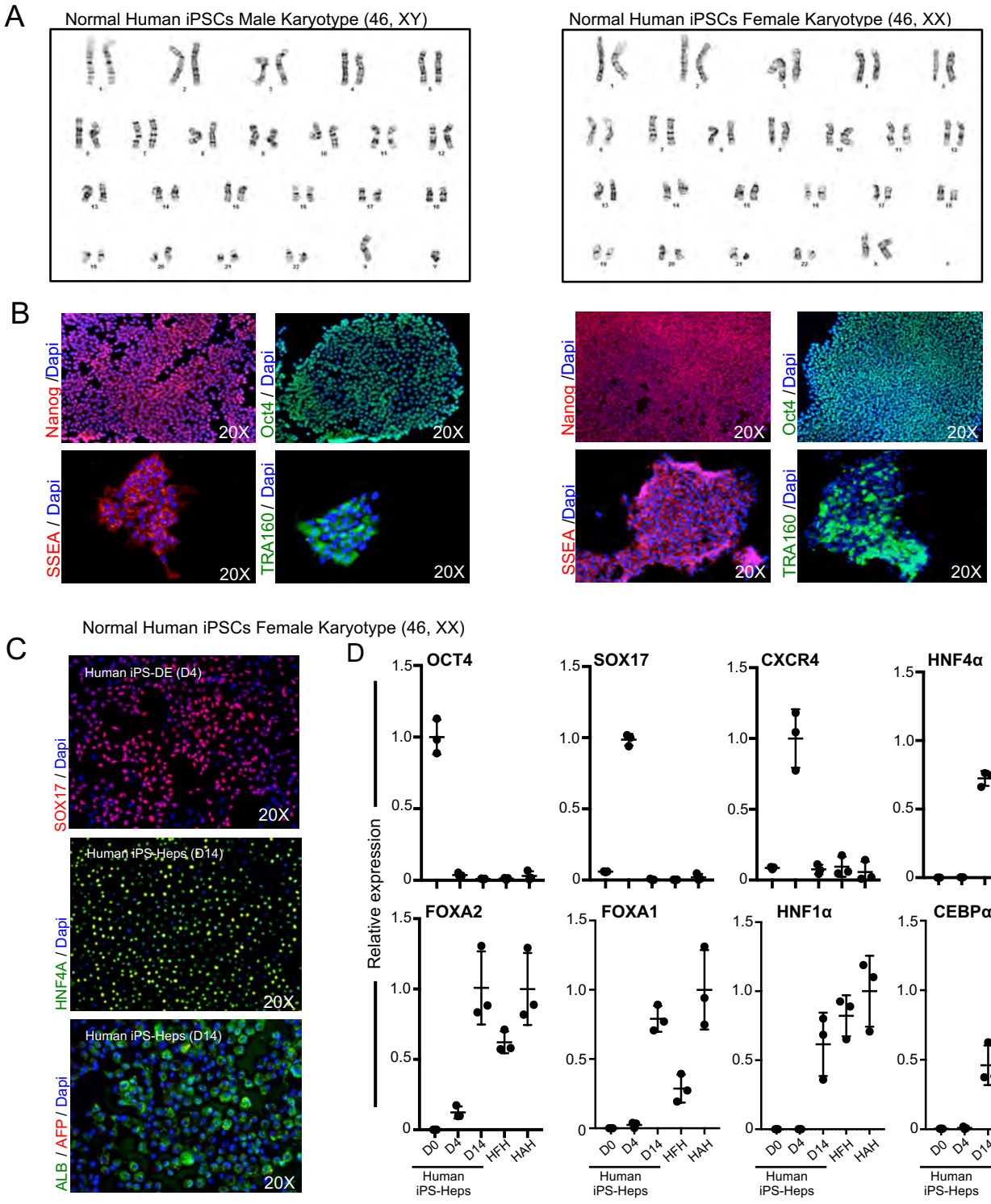

Supplemental Figure 4. Related to STAR Methods. (A) The karyotype of normal human induced pluripotent stem cells (iPSCs) Male (left) and Female (right) used in this study. **(B)** Immunofluorescent staining showing the key marker of pluripotency, such as Nanog, octamer-binding transcription factor (Oct) 3/4, stage-specific embryonic antigen (SSEA), and TRA160. **(C)** Immunofluorescence analyses of the cells derived from induced pluripotent stem cells (iPSCs) of Female Karyotype demonstrating the expression of key definitive endoderm (DE) at day 4 and hepatocyte markers at day14 using antibodies that recognized SRY-BOX (SOX)-17, hepatocyte nuclear factor (HNF) 4α, alpha-fetoprotein (AFP), and albumin (ALB). Dapi, 4',6-diamidino-2-phenylindole dihydrochloride. **(D)** Gene expression profile of human iPSC-derived hepatocytes (iPS-Heps). Data are expressed as the fold change relative to human fetal hepatocytes (HAH), which is set as 1. HFH, human fetal hepatocytes (Gestational age; week 22). Results are representative of three independent differentiation experiments. Error bars represent ± the SD of three independent experiments.

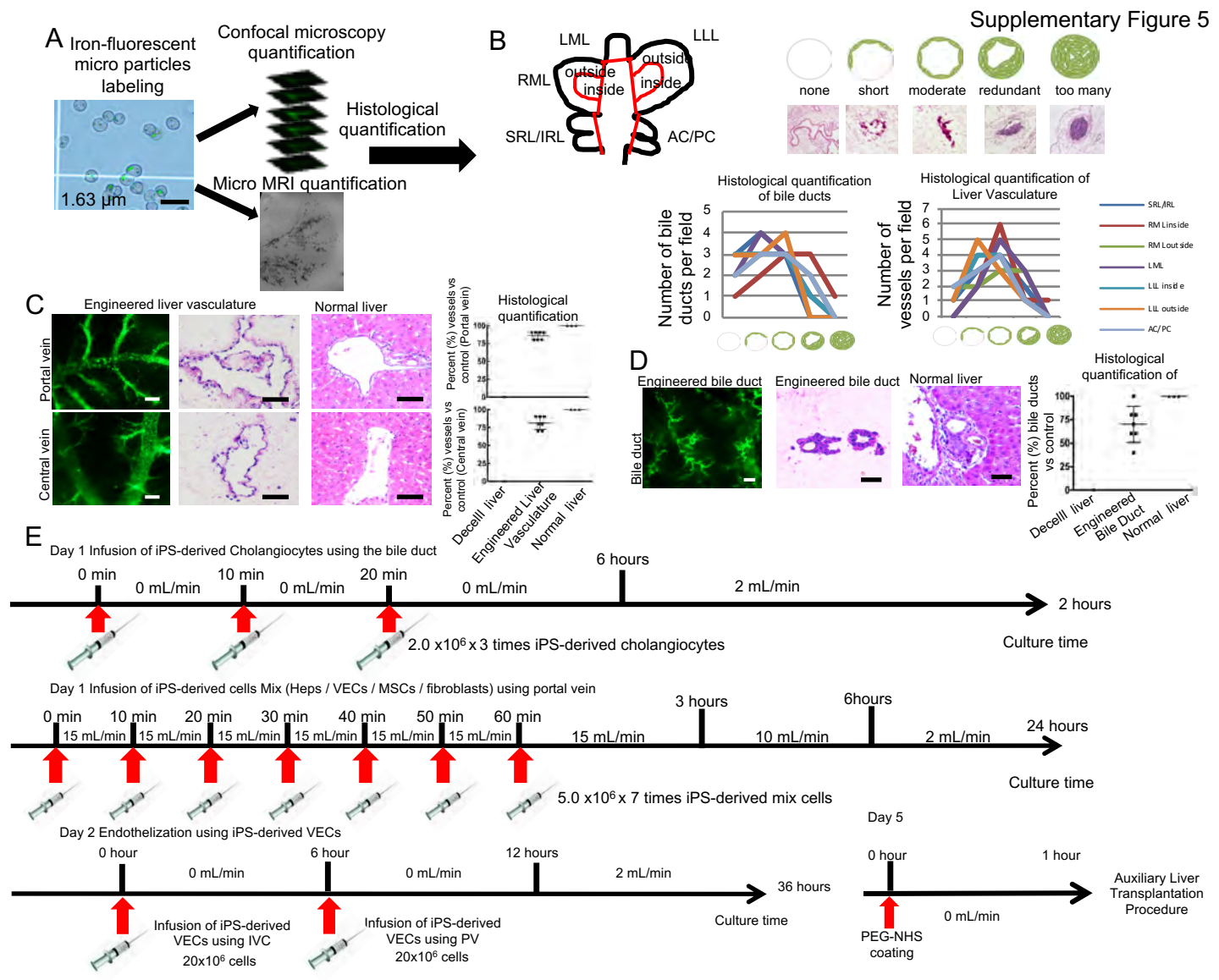

Supplemental Figure 5. Imaging and histological quantitative assessment of vascular and bile duct system assembly. Related to Figure 3,4 and 5. (A) Schematic representation of two different types of anatomical remodeling after repopulation of the vascular and bile duct systems using micron-sized iron oxide particle-labeled endothelial cells and cholangiocytes. An example for quantitative analysis is shown for the biliary tree assembled in the decellualrized rat liver. The rat liver lobes were divided and images of each lobe were obtained by either confocal microscopy or micro-MRI, major branches of the biliary tree were selected, manually traced, and at least 5 different depths images were analyzed at each branch point. The surface area of each bile duct segment was compared to paired images at the same depth and positioning of three-dimensional microCT images of the intrahepatic biliary of normal rat livers that were produced by injecting contrast agent for biliary tree visualization into the common bile duct as described in detail in Methods. **(B)** Schematic representation of the histological quantification of repopulation of bile ducts and vasculature (portal or central vein). The entire repopulated rat liver was divided into different sections for evaluation purposes; superior right lobe (SRL), inferior right lobe (IRL), right medial lobe "outside" or "inside" (RML), left medial lobe (LML), left lateral lobe "outside" or "inside" (LLL), anterior caudate lobe (AC) and posterior caudate lobe (PC). H&E sections of each lobe were traced manually and assigned a level of coverage (none, short, moderate, redundant, too many) and quantified per field. An example of quantitative histological analysis is shown. **(C)** Representative fluorescent confocal microscopy images of the micron-sized iron oxide particle–labeled liver endothelial cells (TMNK-1) in assembled portal and central veins of decellularized livers and the corresponding images of histological sections stained with hematoxylin and eosin. Histological quantification of assembled whole organ vasculature is also shown. Recellularization of portal vein or central vein were performed separately and compared with quantified vasculature from normal liver sections for each lobe. Scale bars: from left to right 100 µm and 50 µm for hematoxylin and eosin photographs. **(D)** Representative fluorescent confocal microscopy images of the micron-sized iron oxide particle-labeled cholangiocytes (MMNK-1) assembled bile duct of decellularized livers and the corresponding images of histological sections stained with hematoxylin and eosin. Histological quantification of assembled whole organ bile ducts is also shown. Scale bars: from left to right 100 µm and 50 µm for hematoxylin and eosin (H&E) photographs. **(E)** Protocols for assembly of liver grafts for transplantation protocol using induced pluripotent stem cells (iPS) derived cells.

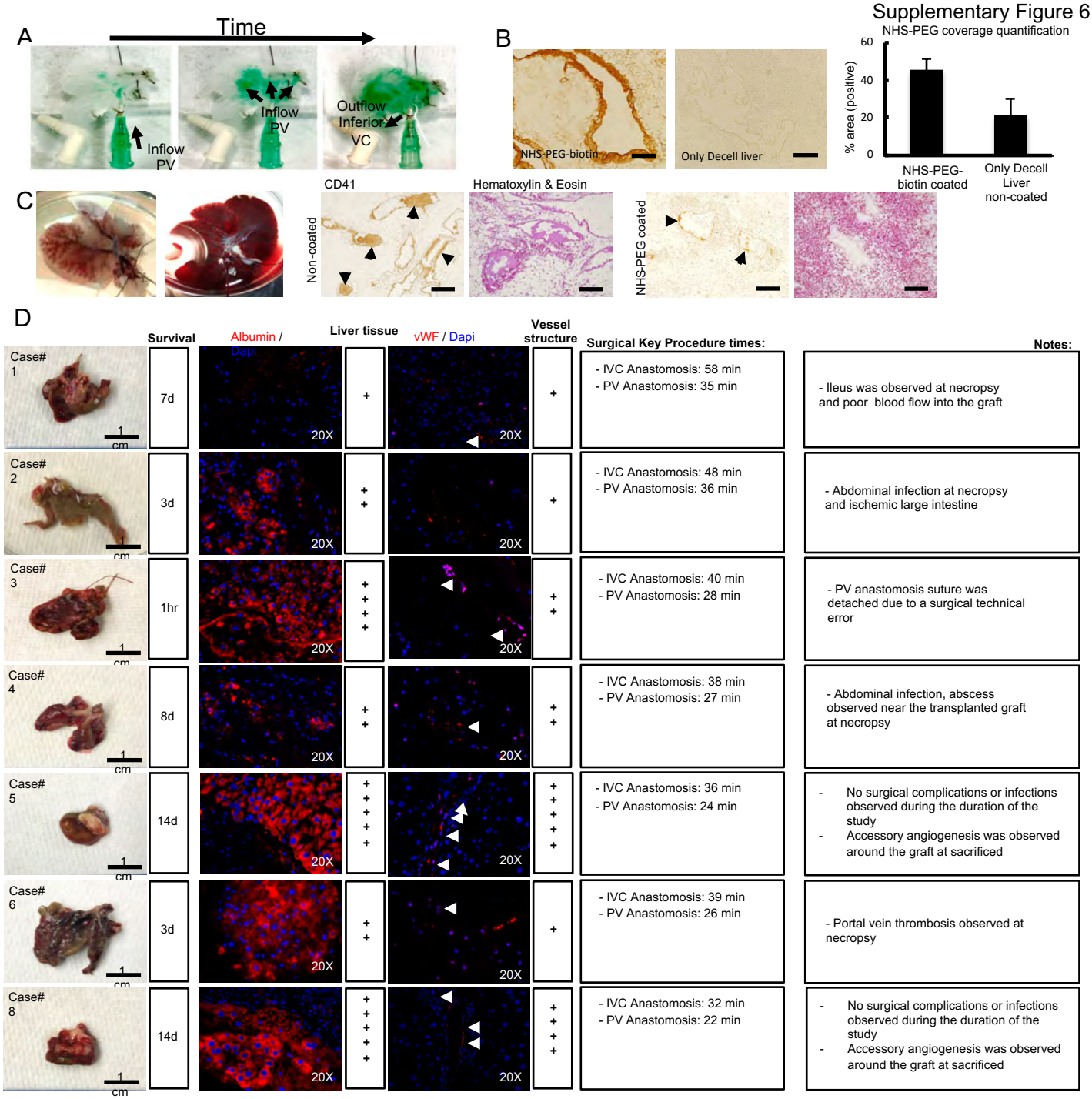

Supplemental Figure 6. Vascular flow direction and effect of NHS-PEG on assembled vasculature in decellularized rat livers and mortality/morbidity analysis of rat primary cells bioengineered liver graft auxiliary transplantation. . Related to Figure 6. (A) Sequential photographs of flow perfusion (green ink perfusate) in bioengineered rat liver grafts, inflow through portal vein (PV) and outflow through inferior vena cava (VC). **(B)** Decellularized liver matrix treated with NHS-PEG-biotin and histological quantification of vessels covered with NHS-PEG-biotin comparing to only decellularized liver non-coated. Bars represent the mean ± the SD of 7 independent experiments. **(C)** Representative photographs of NHS-PEG treated decellularized livers and directly perfused with portal blood flow (left). Immunostaining staining for CD41 (platelet marker) and Hematoxylin & eosin staining of non-coated and NHS-PEG treated decellularized liver matrix after perfusion of portal blood flow. Scale bars: 50 µm (A) 100 µm (C). **(D)** Representative photographs of gross morphology of engineered liver grafts after auxiliary liver transplantation in naïve and liver regeneration conditioned (retrorsine-treated) rats. Immunohistochemical staining of engineered liver grafts after auxiliary liver transplantation left to right: albumin (red), Von Willebrand (vW) factor (red). Arrows head point to vascular structures. Sections were counterstained with DAPI (blue). Also included are surgery key procedures times and notes for each case postmortem analysis. Note: Case#7, bioengineered graft was injured during surgical manipulation before vascular anastomosis.